



## Development of a two-band enhanced vegetation index without a blue band

Zhangyan Jiang<sup>a,\*</sup>, Alfredo R. Huete<sup>a</sup>, Kamel Didan<sup>a</sup>, Tomoaki Miura<sup>b</sup>

<sup>a</sup> Department of Soil, Water, and Environmental Science, University of Arizona, Tucson, AZ, 85721, USA

<sup>b</sup> Department of Natural Resources and Environmental Management, College of Tropical Agriculture and Human Resources, University of Hawaii at Manoa, Honolulu, HI 96822, USA

### ARTICLE INFO

#### Article history:

Received 11 July 2007

Received in revised form 2 June 2008

Accepted 6 June 2008

#### Keywords:

Vegetation indices

EVI

EVI2

Linearization

MODIS

### ABSTRACT

The enhanced vegetation index (EVI) was developed as a standard satellite vegetation product for the Terra and Aqua Moderate Resolution Imaging Spectroradiometers (MODIS). EVI provides improved sensitivity in high biomass regions while minimizing soil and atmosphere influences, however, is limited to sensor systems designed with a blue band, in addition to the red and near-infrared bands, making it difficult to generate long-term EVI time series as the normalized difference vegetation index (NDVI) counterpart. The purpose of this study is to develop and evaluate a 2-band EVI (EVI2), without a blue band, which has the best similarity with the 3-band EVI, particularly when atmospheric effects are insignificant and data quality is good. A linearity-adjustment factor  $\beta$  is proposed and coupled with the soil-adjustment factor  $L$  used in the soil-adjusted vegetation index (SAVI) to develop EVI2. A global land cover dataset of Terra MODIS data extracted over land community validation and FLUXNET test sites is used to develop the optimal parameter ( $L$ ,  $\beta$  and  $G$ ) values in EVI2 equation and achieve the best similarity between EVI and EVI2. The similarity between the two indices is evaluated and demonstrated with temporal profiles of vegetation dynamics at local and global scales. Our results demonstrate that the differences between EVI and EVI2 are insignificant (within  $\pm 0.02$ ) over a very large sample of snow/ice-free land cover types, phenologies, and scales when atmospheric influences are insignificant, enabling EVI2 as an acceptable and accurate substitute of EVI. EVI2 can be used for sensors without a blue band, such as the Advanced Very High Resolution Radiometer (AVHRR), and may reveal different vegetation dynamics in comparison with the current AVHRR NDVI dataset. However, cross-sensor continuity relationships for EVI2 remain to be studied.

© 2008 Elsevier Inc. All rights reserved.

### 1. Introduction

Satellite vegetation index (VI) products are commonly used in a wide variety of terrestrial science applications that aim to monitor and characterize the Earth's vegetation cover from space (e.g. Myneni et al., 1997a; Saleska et al., 2007). VIs are optical measures of vegetation canopy "greenness", a composite property of leaf chlorophyll, leaf area, canopy cover, and canopy architecture. Although VIs are not intrinsic physical quantities, they are widely used as proxies in the assessment of many biophysical and biochemical variables, including canopy chlorophyll content (Blackburn, 1998; Gitelson et al., 2005), leaf area index (LAI) (e.g. Boegh et al., 2002; Chen & Cihlar, 1996), green vegetation fraction (e.g. Gutman & Ignatov, 1998; Jiang et al., 2006a; Zeng et al., 2000), gross primary productivity (GPP) (Rahman et al., 2005; Sims et al., 2006), and fraction of photosynthetically active radiation absorbed by the vegetation (FAPAR) (e.g. Di Bella et al., 2004; Myneni et al., 1997b).

As global climate and land use/land cover changes are occurring at unprecedented rates, long-term consistent and continuous satellite data records are desperately needed to monitor and quantify changes to the global environment. VI time series data records have played an

important role in measuring and characterizing land surface responses to climate variability and change (e.g. Heumann et al., 2007; Tucker et al., 2001). Normalized difference vegetation index (NDVI) time series data products based on the Advanced Very High Resolution Radiometer (AVHRR) instruments, such as the GIMMS (Global Inventory Modeling and Mapping Studies) and Pathfinder AVHRR Land (PAL) datasets, are available from 1981, and have contributed significantly to global land processes studies, vegetation–climate interactions, and other advancements in Earth System Science (e.g. Defries & Belward, 2000; Suzuki et al., 2007; Townshend, 1994; Tucker et al., 1986).

However, it remains a challenge to produce long-term and consistent vegetation index time series across sensor systems with variable spectral response functions, spatial resolution, swath width and orbiting geometry. Degradations in the AVHRR instrument gain values and drifts in the calibration coefficients may result in significant errors in VI time series computed from prelaunch calibration values (e.g. Che & Price, 1992; Kaufman & Holben, 1993). Numerous investigations have evaluated NDVI continuity, and proposed NDVI inter-sensor translation equations, across AVHRR sensors (e.g. Los, 1993; Roderick et al., 1996) as well as between AVHRR and more recent sensors, including the Moderate Resolution Imaging Spectroradiometer (MODIS), the System Pour l'Observation de la Terre (SPOT)-VEGETATION, the Sea-viewing Wide Field-of-view Sensor (SeaWiFS), the Landsat Enhanced Thematic

\* Corresponding author.

E-mail address: [zjiang@email.arizona.edu](mailto:zjiang@email.arizona.edu) (Z. Jiang).

Mapper (ETM+), the Medium Resolution Imaging Spectrometer (MERIS) and the Visible/Infrared Imager Radiometer Suite (VIIRS) (Brown et al., 2006; Fensholt et al., 2006; Gallo et al., 2005; Gitelson & Kaufman, 1998; Günther & Maier, 2007; Miura et al., 2006; Steven et al., 2003; Tucker et al., 2005; van Leeuwen et al., 2006; Yoshioka et al., 2003).

VIs from MODIS instruments represent improved spatial, spectral, and radiometric measurements of surface vegetation conditions (Tucker et al., 2005). There are currently two vegetation index standard products generated with data from the Terra and Aqua MODIS instruments, NDVI and the enhanced vegetation index (EVI), with the EVI utilizing a blue band in addition to the red and NIR bands. In comparison to NDVI, EVI was found to be more linearly correlated with green leaf area index (LAI) in crop fields (Boegh et al., 2002), less prone to saturation in temperate and tropical forests (Huete et al., 2006; Xiao et al., 2004), and minimally sensitive to residual aerosol contamination from extensive fires in the Amazon and Northern Asia (Miura et al., 1998; Xiao et al., 2003).

Although there are many studies investigating cross-sensor continuity of NDVI, investigations on EVI cross-sensor translation are quite few. Fensholt et al. (2006) suggested that the consistency of EVI values across different sensors might be more problematic due to more difficult and varying atmospheric correction schemes of the blue band. There are almost 9 years of MODIS EVI time series available since 2000. The extension of the EVI time series, back to 1981 with the historical AVHRR data, is desirable but difficult since EVI is limited to sensor systems designed with a blue band, in addition to the red and near-infrared bands.

However, since the role of the blue band in EVI does not provide additional biophysical information on vegetation properties, but rather is aimed at reducing noise and uncertainties associated with highly variable atmospheric aerosols, a 2-band adaptation of EVI should be compatible. Although a 2-band EVI (EVI2) would be computed without a blue band, it would remain functionally equivalent to EVI, although slightly more prone to aerosol noise, which is becoming less significant with continuing advancements in atmosphere corrections.

The purpose of this study is to develop and evaluate a 2-band EVI, without a blue band, which has the best similarity with the 3-band EVI, particularly when atmospheric effects are insignificant and data quality is good. The overall aim for EVI2 is to maintain the soil-adjustment and linearization functions in EVI. In this way EVI2 can be used as an acceptable substitute of EVI over atmospherically corrected and good quality pixels. The development of EVI2 would enable extension of EVI to instruments without a blue band, such as AVHRR and the Advanced Spaceborne Thermal Emission and Reflection Radiometer (ASTER), for cross-sensor applications and for generating a backward compatibility of EVI to the historical AVHRR record, thus complementing the NDVI long-term record.

This paper is organized to first provide a brief review of the VIs of concern to this study, followed by a conceptual approach to the development of a new vegetation index, the linear vegetation index (LVI), which is calibrated to fit EVI and labeled EVI2. Our data and methods are chosen to achieve a globally-representative diverse set of landscape conditions to achieve the best similarity between EVI2 and EVI. The EVI2–EVI consistency is evaluated and demonstrated spatially and temporally at global and local scales. Differences and similarities between EVI2 and other VIs are then discussed and summarized.

## 2. Brief review of vegetation indices

NDVI is defined by:

$$\text{NDVI} = \frac{N-R}{N+R} \quad (1)$$

where  $N$  and  $R$  are the reflectances in the near-infrared (NIR) and red bands. Despite the usefulness of NDVI data in vegetation studies, it

does have some limitations related to soil background brightness, in which separate NDVI relationships with canopy biophysical properties are found over different soil and moisture conditions (Bausch, 1993; Elvidge, & Lyon, 1985; Huete et al., 1985). In order to overcome this problem, Huete (1988) proposed using a soil-adjustment factor,  $L$ , to account for first-order, non-linear, differential NIR and red radiative transfer through a canopy, and obtained a soil-adjusted vegetation index (SAVI),

$$\text{SAVI} = (1+L) \frac{N-R}{N+R+L} \quad (2)$$

Several modifications have been made to the SAVI equation, and the transformed SAVI (TSAVI) (Baret & Guyot, 1991; Baret et al., 1989), modified SAVI (MSAVI) (Qi et al., 1994), optimized SAVI (OSAVI) (Rondeaux & Baret, 1996), and generalized SAVI (GESAVI) (Gilbert et al., 2002) were subsequently proposed.

NDVI is also sensitive to attenuation and scattering by the atmosphere from highly variable aerosols (Ben-Ze'ev et al., 2006; Carlson & Ripley, 1997; Kaufman & Tanré, 1992; Miura et al., 1998). The atmospherically resistant vegetation index (ARVI) was proposed by Kaufman and Tanré (1992) in which aerosol effects are self-corrected by using the difference in blue and red reflectances to derive the surface red reflectance. Another approach to minimize atmospheric effects on NDVI is to use the middle-infrared wavelength region (1.3–2.5  $\mu\text{m}$ ) as a substitute for the red band since longer wavelengths are much less sensitive to smoke and aerosols (Karnieli et al., 2001; Miura et al., 1998).

Finally, NDVI is non-linear and saturates in high biomass vegetated areas (e.g. Gitelson, 2004; Huete et al., 2002; Ünsalan & Boyer, 2004). The sensitivity of NDVI to leaf area index (LAI) becomes increasingly weak with increasing LAI beyond a threshold value, which is typically between 2 and 3 (Carlson & Ripley, 1997). Reduction of saturation effects and improved linearity adds to the observed accuracy in estimating biophysical parameters from the VI values and provides a mechanism for multi-sensor (resolution) scaling of VI values (Huete et al., 2002).

Several methods have been reported recently to overcome the saturation effects on NDVI. Ünsalan and Boyer (2004) proposed to transform NDVI by using an inverse tangent function. However, a sensitivity analysis found the transformed NDVI cannot improve sensitivity to vegetation at vegetation fractions larger than 0.6 (Jiang et al., 2006b). Gitelson (2004) and Vaiopoulos et al. (2004) further proposed adding weighting factors to the NIR reflectance term in the NDVI equation to adjust the relative contributions of the NIR and red reflectances to NDVI. However, these weighting factors did not address the influence of soil background and they altered the dynamic range of NDVI, resulting in a range between  $-0.6$  and  $0.6$  (Gitelson 2004).

EVI was developed to optimize the vegetation signal with improved sensitivity in high biomass regions and improved vegetation monitoring through a de-coupling of the canopy background signal and a reduction in atmosphere influences:

$$\text{EVI} = G \frac{N-R}{N+C_1R-C_2B+L} \quad (3)$$

where  $N$ ,  $R$ , and  $B$  are atmospherically corrected or partially atmosphere-corrected (Rayleigh and ozone absorption) surface reflectances in near-infrared, red and blue bands respectively;  $G$  is a gain factor;  $C_1$ ,  $C_2$  are the coefficients of the aerosol resistance term, which uses the blue band to correct for aerosol influences in the red band, and  $L$  functions as the soil-adjustment factor as in SAVI (Eq. (2)), but its value is different from the  $L$  in SAVI, attributed to the interaction and feedbacks between the soil-adjustment factor and the aerosol resistance term (Liu & Huete, 1995). The coefficients adopted in the MODIS EVI algorithm are,  $L=1$ ,  $C_1=6$ ,  $C_2=7.5$ , and  $G=2.5$ . EVI has been used recently in a wide variety studies, including those on land cover/land cover change (Wardlow et al., 2007), estimation of vegetation biophysical parameters (Chen et al.,

2004; Houborg et al., 2007), phenology (Ahl et al., 2006; Xiao et al., 2006; Zhang et al., 2003), evapotranspiration (Nagler et al., 2005), biodiversity (Waring et al., 2006), and the estimation of gross primary production (GPP) (Rahman et al., 2005; Sims et al., 2008, 2006).

EVI not only gains its heritage from SAVI and ARVI, but also improves the linearity with vegetation biophysical parameters, encompassing a broader range in LAI retrievals (Houborg et al., 2007). It has also been shown to be strongly linear related and highly synchronized with seasonal tower photosynthesis measurements in terms of phase and amplitude, with no apparent saturation observed over temperate evergreen needleleaf forests (Xiao et al., 2004), tropical broadleaf evergreen rainforests (Huete et al., 2006), and particularly temperate broadleaf deciduous forests (Rahman et al., 2005; Sims et al., 2006). Deng et al. (2007) found that EVI was effective in vegetation monitoring, change detection, and in assessing seasonal variations of evergreen forests. Wardlow et al. (2007) found that NDVI began to approach an asymptotic level at the peak of the growing season over cropland, whereas EVI exhibited more sensitivity during this growth stage.

### 3. Derivation of a 2-band EVI

The main concept of the SAVI is that vegetation biophysical isolines in NIR-red reflectance space, i.e., lines in a spectral space corresponding to constant vegetation amount (e.g. LAI, chlorophyll content, biomass) and canopy structure (e.g., canopy shape, leaf angle distribution) but varying pixel brightness caused by the variation of soil background brightness, are neither parallel to a soil line as in the case of perpendicular vegetation index (PVI) isolines (Richardson & Wiegand, 1977), nor converge at the origin as in the case of NDVI isolines, but instead, approximately converge at a point on a simplified soil line ( $Y=X$ ) shifted from the origin in the negative direction (Jiang et al., 2006b; Huete 1988). For various crop canopies and a wide range of vegetation amounts, the convergence point was approximately at point E  $(-l, -l)$  (Fig. 1). Vegetation biophysical isoline behavior was modeled graphically by SAVI isolines through shifting of the NIR-red reflectance space origin toward the isoline convergence point E, and a new coordinate system, Red'-NIR', is created, with Red' and NIR' coordinates denoted as  $R'$  and  $N'$ , respectively (Fig. 1). Shifting the origin toward negative values is equivalent to adding an offset or

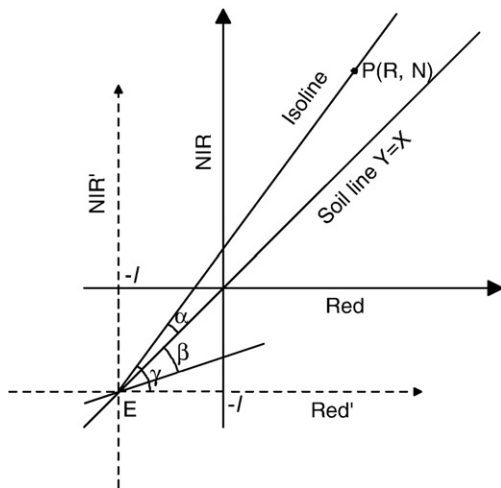


**Fig. 1.** The isolines of SAVI and the soil-adjusted simple ratio (SASR) and their angles in red-NIR reflectance space. Any lines crossing point E is a SAVI isoline as well as a SASR isoline according to its definition (Huete, 1988). Any given point P (R, N) in red-NIR space corresponds to a unique SAVI/SASR isoline, PE. A new coordinate system, Red'-NIR', is created by shifting the origin of the red-NIR coordinate system to point E. The coordinate of point P in the new coordinate system ( $R', N'$ ) equals to  $(R+l, N+l)$ .  $\alpha$  is the angle between a simplified soil line ( $Y=X$ ) and the SAVI/SASR isoline, PE.  $\beta$  describes a line across E deviating from the soil line in the clockwise direction, varying between 0 and  $\pi/4$ .  $\gamma$  is the angle between PE and the Red' axis.

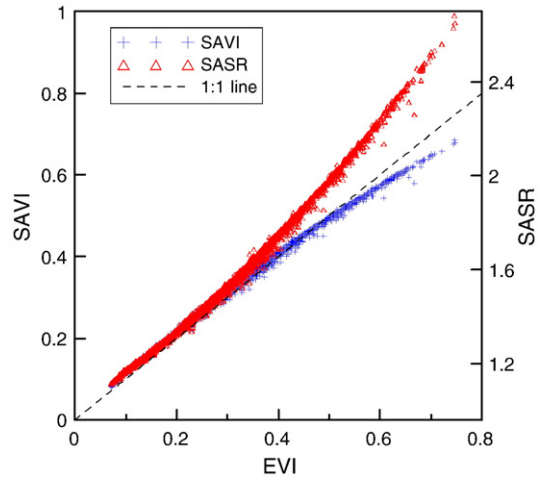


**Fig. 2.** Relationships between EVI with SAVI and SASR generated from MODIS data as described in Section 4.1.

constant,  $l$ , to the red and NIR reflectance values, i.e.  $N'=N+l$ , and  $R'=R+l$ , such that the simple ratio (SR) and NDVI become

$$\frac{N'}{R'} = \frac{N+l}{R+l} \tag{4}$$

and

$$\frac{N'-R'}{N'+R'} = \frac{N-R}{N+R+2l}, \tag{5}$$

respectively (Huete, 1988). In order to maintain the amplitude of Eq. (5) as that of NDVI, a gain,  $(1+L)$ , is multiplied to Eq. (5), such that the SAVI equation is obtained (Eq. (2)), where  $L=2l$ . In this paper, Eq. (4) is denoted as a soil-adjusted SR (SASR). The  $L$  value is usually determined as 0.5 and thus  $l=0.25$ .

Fig. 2 presents the relationships between SAVI, SASR and EVI generated from high quality assurance (QA) MODIS data, i.e., atmosphere-corrected pixels with initially low aerosol quantities (the description of these data is in Section 4.1). Since the three indices are soil-adjusted VIs, SAVI and SASR are related to EVI very well, with small EVI variations corresponding to each SAVI and SASR values. These variations are mostly caused by the variation of the blue band since EVI values depend on the blue reflectance in addition to the red and NIR reflectances. However, both VIs are not linearly related to EVI across all vegetation density levels. When EVI is less than 0.5, the values of SAVI are similar to EVI values, but SAVI become less sensitive than EVI over more highly vegetated regions. In contrast, SASR is more sensitive than EVI when EVI is larger than 0.3.

Recently, Jiang et al. (2006b) showed that many vegetation indices are functions of spectral angles related to their VI isolines in NIR-red reflectance space, and SAVI can be expressed as,

$$\text{SAVI} = (1+L) \tan(\alpha) \tag{6}$$

where  $\alpha$  is the angle between the simplified soil line and a SAVI isoline as indicated in Fig. 1. So  $\alpha$  can be expressed by,

$$\alpha = \arctan(\text{SAVI}/(1+L)) \tag{7}$$

The SASR also can be expressed as a tangent function of angles,

$$\text{SASR} = \tan(\gamma) = \tan(\alpha + \pi/4) \tag{8}$$

where  $\gamma$  is the angle between a SASR isoline (same as the SAVI isoline) and the horizontal red' axis (Fig. 1). Thus the relationship between SAVI and the SASR is

$$\text{SASR} = \tan[\arctan(\text{SAVI}/(1+L)) + \pi/4] \tag{9}$$

The SASR is a non-linear transform of SAVI, through which the convex SAVI–EVI relationship is converted to the concave SASR–EVI relationship (Fig. 2). A linear vegetation index (LVI) comparable to EVI can be obtained by adjusting the constant angle  $\pi/4$  to a variable angle  $\beta$  in Eq. (9),

$$\text{LVI}(\beta) = \tan[\arctan(\text{SAVI}/(1+L)) + \beta] \quad (10)$$

where  $\beta$  describes a line across E deviating from the soil line in the clockwise direction in Fig. 1. LVI is equivalent to SASR when  $\beta=\pi/4$ , and equivalent to SAVI when  $\beta=0$ . The LVI value of the soil line,  $Y=X$ , ( $\text{LVI}_0$ , corresponding to  $\alpha=0$ ) is

$$\text{LVI}_0 = \tan(\beta) \quad (11)$$

By subtracting  $\text{LVI}_0$  from Eq. (10) and multiplying a gain,  $G'$ , in order to maintain the amplitude of LVI as that of EVI, LVI becomes (Appendix A)

$$\text{LVI} = G'[\tan(\alpha + \beta) - \tan\beta] = G \frac{N-R}{N + R \tan(\pi/4 + \beta) + L/(1 - \tan\beta)} \quad (12)$$

where

$$G = \frac{G' \sec^2\beta}{(1 - \tan\beta)} \quad (12 - 1)$$

$\beta$  acts as a linearity-adjustment factor since the linearization of LVI with respect to a VI or a biophysical parameter can be achieved by adjusting the value of this angle. With optimal  $L$ ,  $\beta$  and  $G$ , the differences between the LVI values and the EVI values would be very small when atmospheric effects are insignificant and no snow/ice and residual cloud are present in pixels, and this optimal LVI is denoted as the 2-band EVI, i.e. EVI2 in this paper.

An alternative method to develop EVI2, rather than based on LVI, is to decompose the EVI equation (Eq. (3)) into a 2-band EVI by relating the blue band to the red band. Using the airborne visible-infrared imaging spectrometer (AVIRIS) data, Clevers (1999) found visible bands are highly related to each other over agriculture fields. Kaufman et al. (1997) and Karnieli et al. (2001) found that under clear sky conditions, the SWIR spectral bands are highly correlated with the visible (blue, green and red) spectral bands over various land covers. So the visible bands should be highly correlated to each other, enabling the blue reflectance to be expressed as a function of the red reflectance at the ground level. By simply assuming the relationship,  $\text{Red} = c \times \text{Blue}$ , the EVI equation can be reduced to a 2-band EVI using the  $L$ ,  $C_1$ , and  $C_2$  values mentioned above,

$$\text{EVI2} = G \frac{N-R}{N + (6-7.5/c)R + 1} \quad (13)$$

where  $G$  is to be determined according to the  $c$  value. It should be noted that  $c$  derived by fitting the blue reflectance to the red reflectance might not necessarily be the same as that derived by fitting EVI2 to EVI since NIR reflectances are involved in fitting EVI2 to EVI but not used to relating the blue reflectance to the red reflectance.

## 4. Data and methods

### 4.1. Data for EVI2 calibration

#### 4.1.1. Site choice

MODIS data over 40 globally distributed sites, representing a wide variety of land cover conditions are used to derive optimal parameters for EVI2. These sites include 19 Earth Observation System (EOS) Land Validation core sites (<http://landval.gsfc.nasa.gov>), 19 Ameriflux tower sites (<http://public.ornl.gov/ameriflux/>), and 2 additional, sparsely vegetated sites to obtain a full representation of land surfaces. The sites represent a wide range of fairly homogeneous land cover types at scales consistent with satellite observations, and with a well-

documented history of *in situ* measurements and canopy characterization (Morissette et al., 2002).

The EOS Land Validation Core Sites were primarily designed to aid in satellite land product validation over a wide range of biome types, and provide *in situ* measurements as well as aircraft data in support of EOS instruments and long-term satellite measurements (Morissette et al., 2002). Ameriflux is part of FLUXNET, a global network of micrometeorological sites providing continuous measurements of water vapor and carbon dioxide fluxes between atmosphere and terrestrial ecosystems. This network also provides ecological site data and remote sensing products.

The two other sites, Tinga Tingana, Australia and Tshane, Botswana, are characterized by sparse vegetation and were chosen to encompass a complete range of land surfaces and corresponding optical properties, red and NIR reflectances, and brightness values. The Tinga Tingana region lies within the Strzelecki Desert in South Australia and was used as an EO-1 Hyperion validation site (<http://hl2.bgu.ac.il/users/www/9451/HIS/HIS/Hyperion.htm>). This site consists of light colored sand dunes with less than 5% vegetation (Mitchell et al., 1997). Tshane is a test site of the Southern African Regional Science Initiative Project (SAFARI 2000) (<http://www-eosdis.ornl.gov/S2K/safari.html>) and a land product validation (LPV) site of the Committee on Earth Observing Satellites (CEOS) ([http://lpvs.gsfc.nasa.gov/LPV\\_CS\\_gen.php](http://lpvs.gsfc.nasa.gov/LPV_CS_gen.php)). This site is located approximately 15 km south of Tshane, Botswana and has a vegetation cover of open savanna dominated by *Acacia luederitzii* and *A. mellifera* with an overstory height of about 7 m (Privette et al., 2002).

#### 4.1.2. Data extracts

MODIS 1 km, 16-day composite Vegetation Index product (MOD13A2), from Collection 4 and the Terra platform, are extracted over the 40 sites, from 18 February 2000 to 19 December 2005. The MODIS standard VI products include two, gridded vegetation indices (NDVI, EVI), product quality assessment (QA), input red (band 1), near-infrared (NIR) (band 2), blue (band 3), and middle-infrared (MIR) (band 7) reflectances, and sensor view, solar zenith and relative azimuth angles for each pixel (Huete et al., 2002). A window of  $3 \times 3$  pixels, centered on the location of each site, is used to extract red, NIR and blue reflectances over each site. Only good quality pixels are used to generate the average reflectances of each window, from which the VI values are calculated for each site at 16-day intervals. Good quality pixels are defined as those with VI usefulness index  $\leq 0010$  (i.e., the best 3 levels among 16 quality assurance (QA) levels), aerosol quantity  $\leq 01$  (low aerosol quantity), no mixed clouds, no snow/ice, and no cloud shadow ([http://edcdaac.usgs.gov/modis/moyd13\\_qa\\_v4.asp](http://edcdaac.usgs.gov/modis/moyd13_qa_v4.asp)). Spatially average reflectances are computed for each site and for each composite period, only when the number of good quality pixels in a  $3 \times 3$  subset was larger than or equal to 5. In total, 2898 measurements, or 54% of the 5400 (135 composites for each site) original measurements are of acceptable QA and used in the determination of the optimal parameters in the EVI2 equations (Eqs. (12) and (13)).

### 4.2. Data for evaluation of EVI–EVI2 consistency

In order to evaluate the similarities between EVI2 and EVI globally, a one-year global MODIS 1 km, 16-day composite dataset (collection 5), from Feb. 18, 2000 to Feb. 18, 2001, including 24 global composites, are analyzed. In addition, 13 globally distributed EOS land validation core sites, different from the 40 sites used in the optimization of EVI2 parameters, including a range of biomes are selected for local scale comparisons and evaluation of the different VI time series (<http://landval.gsfc.nasa.gov/>). An average intra-annual profile of QA-accepted VI values from 2000 to 2006 is generated for EVI, EVI2, and NDVI, based on average reflectances of  $3 \times 3$  pixels at each site. The latest reprocessed MODIS data (collection 5) is not significantly different from the previous version (collection 4), with primary differences associated with improvements to the lower quality data (e.g., aerosol

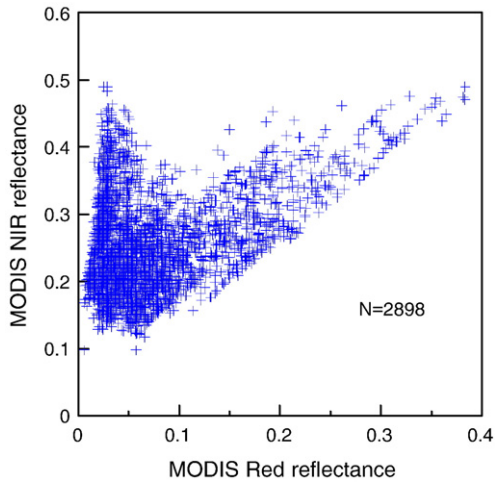


Fig. 3. QA-accepted, 16-day composite red and NIR reflectances over the 40 study sites from 18 February 2000 to 19 December 2005.

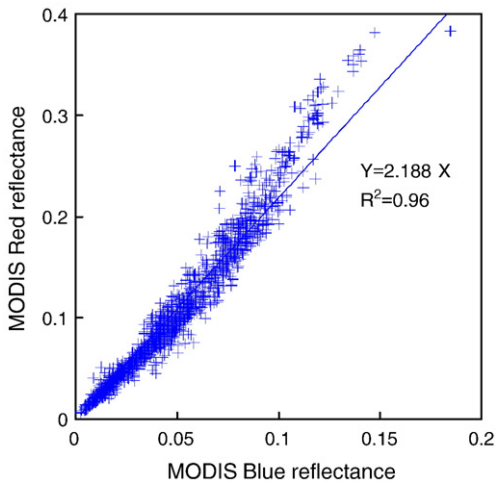


Fig. 4. QA-accepted, 16-day composite blue and red reflectances over the 40 study sites from 18 February 2000 to 19 December 2005.

quality and adjacent cloud filters). These improvements have none or negligible effects on the good quality data extracted in this study and the data consistency between collections 4 and 5 (Didan & Huete, 2006).

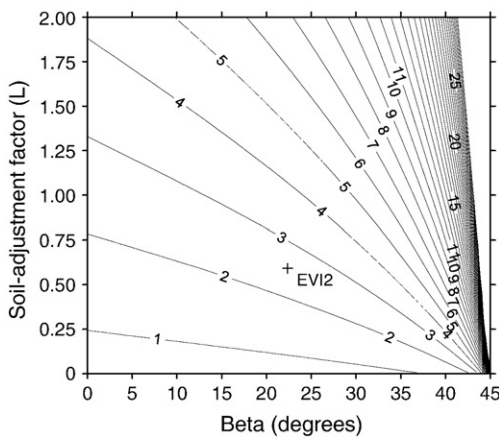


Fig. 5. Optimal G value in EVI2 as a function of  $\beta$  and soil-adjustment factor (L) to maintain the amplitude of EVI2 comparable to that of EVI.

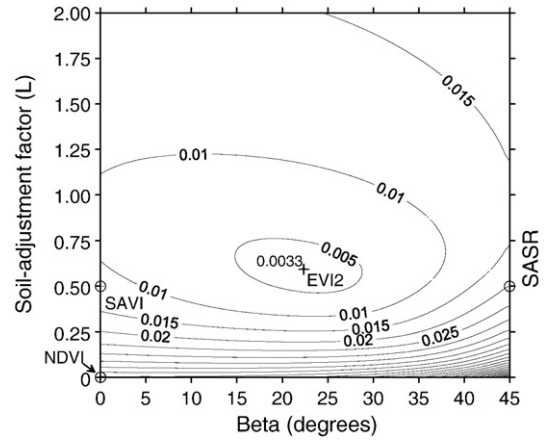


Fig. 6. The mean absolute difference (MAD) between EVI and EVI2 as a function of  $\beta$  and soil-adjustment factor (L) calculated with the optimal G as shown in Fig. 5.

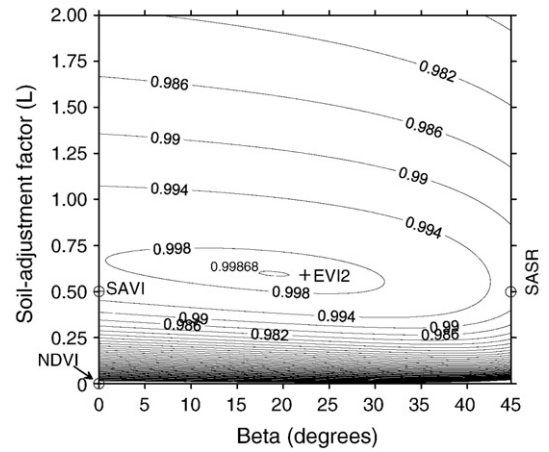


Fig. 7. Coefficient of determination ( $R^2$ ) between EVI and EVI2 as a function of  $\beta$  and soil-adjustment factor (L).

4.3. Methods

EVI2 should have the best similarity with the 3-band EVI when atmospheric effects are insignificant and negligible, and no residual

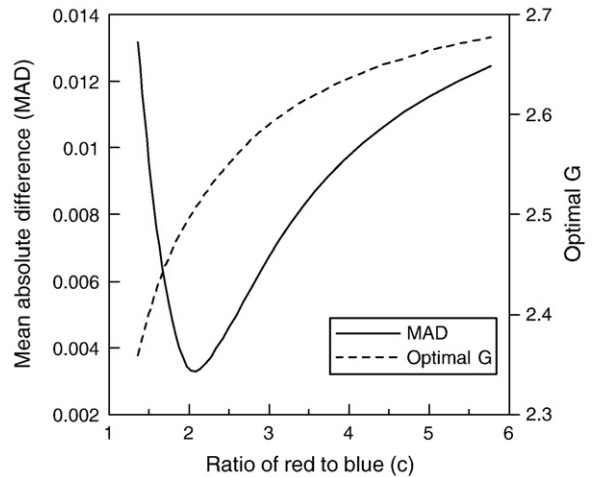
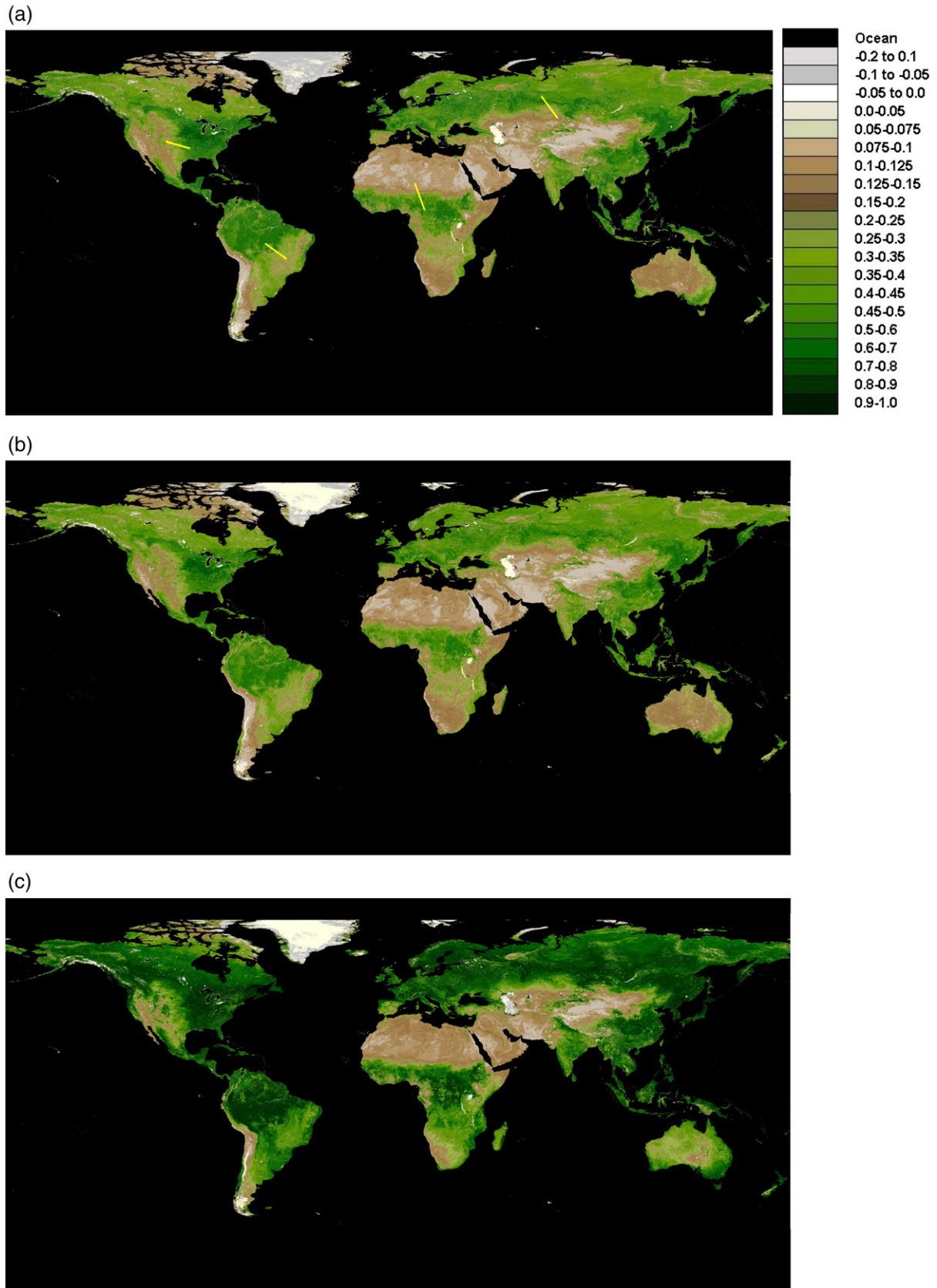


Fig. 8. Mean absolute difference between EVI and EVI2 and the optimal G as functions of the ratio of red to blue reflectances (c) (Eq. (13)).



**Fig. 9.** Comparison of global MODIS 1 km, 16-day composite Vegetation Indices during Jul 27–Aug 11, 2000 (DOY 209–224) composite period, (a) EVI, (b) EVI2, (c) NDVI, (d) EVI2 minus EVI. The legends of (b) and (c) are the same as (a). Four yellow lines in (a) indicate the position of transects varying from sparsely to densely vegetated regions in four continents.

(d)

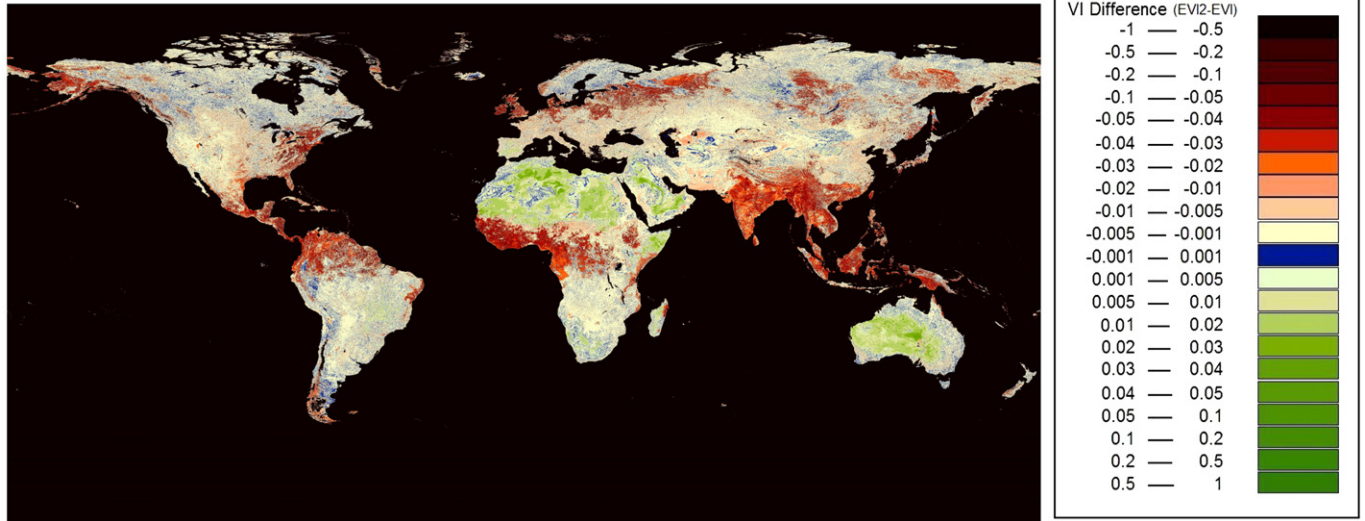


Fig. 9 (continued).

cloud and snow/ice are present in a pixel. The mean absolute difference (MAD) between EVI and EVI2 is used as a measurement of similarity,

$$\text{MAD} = \frac{1}{n} \sum_{i=1}^n |\text{EVI}_i - \text{EVI2}_i| \quad (14)$$

where  $n$  is the total number of measurements used here (2898) and  $i$  denotes each measurement. For a given combination of  $L$  and  $\beta$ , there is a single, optimal  $G$  that minimizes MAD between EVI and EVI2. A dichotomy algorithm is used to search out an optimal  $G$  between 0 and 100 and then MAD is calculated with the optimal  $G$  and the given  $L$ ,  $\beta$  values.  $L$  is increased from 0 to 2 and  $\beta$  from 0 to  $45^\circ$  at increments of 0.01, respectively. As shown in Fig. 1,  $\beta$  varies between 0 and  $\pi/4$ , corresponding to two boundary cases, SAVI and SASR, respectively. Then the minimum MAD, along with the corresponding optimal  $L$ ,  $\beta$  and  $G$  values, can be identified in the  $L$ - $\beta$  space. The coefficient of determination ( $R^2$ ) between EVI and EVI2 is used as a reference of similarity since an optimal EVI2 should be linearly related to EVI, which is also a function of  $\beta$  and  $L$ , but independent on  $G$ . Since MAD takes the variations of  $L$ ,  $\beta$  and  $G$  into account, it is used as the basis of optimization/calibration.

For the decomposition method, there is an optimal  $G$  value for a given  $c$  value, which minimizes MAD between EVI and EVI2 according to Eq. (13). Thus, the optimal  $G$  and MAD are calculated as functions of  $c$  and this enables the minimum MAD and corresponding  $G$  and  $c$  values to be identified.

## 5. Calibration of EVI2

Fig. 3 shows all the QA-accepted, 16-day composite red and NIR reflectances over the 40 study sites from 18 February 2000 to 19 December 2005. The reflectances encompassed a wide range of values, with red reflectances ranging from 0.006 to 0.383 and NIR reflectances from 0.098 to 0.490, which represents reflectances over most surface conditions except snow. A wide range of soil background brightness is included since (1) the 40 sites are selected globally ranging from wet, densely vegetated areas to dry, bright desert areas and (2) various fractions of soil background at each site can be observed temporally over different seasons, particularly within agriculture, shrub, grassland, and deciduous forest sites.

The relationship between red and blue reflectances is highly correlated (Fig. 4) ( $R^2=0.96$ ), described by a regression line of,

red=2.188×blue, which suggests that the blue band does not contribute much additional information about the land surface than the red band at the canopy level and when atmospheric effects are insignificant. This provides a theoretical basis for deriving a 2-band EVI without loss of significant information about the land surface, relative to EVI, when atmospheric effects are insignificant.

When the values of  $L$  and  $\beta$  increase, the denominator of the EVI2 equation (Eq. (12)) increases and thus the amplitude of EVI2 decreases. By using the QA-accepted reflectances, as shown in Figs. 3 and 4, an optimal  $G$  is searched out to achieve the minimum MAD for each combination of  $L$  and  $\beta$ . The optimal  $G$  increases with the increase of  $L$  and  $\beta$  to compensate for the loss of amplitude and maintain the amplitude of EVI2 to that of EVI (Fig. 5). Then MAD between EVI and EVI2 is computed as a function of  $L$  and  $\beta$  with the optimal  $G$  for each combination of  $L$  and  $\beta$  (Fig. 6). MAD decreases rapidly when  $L$  increases for 0 to 0.5, and increases for higher  $L$ . MAD for SAVI at point  $\beta=0$ ,  $L=0.5$  in Fig. 6 is much smaller than MAD for NDVI at point  $\beta=0$ ,  $L=0$ . MAD also varies with  $\beta$ , with intermediate  $\beta$  values resulting in a smaller MAD. The minimum MAD is achieved when  $\beta=22.38^\circ$  ( $\tan(\beta)=7/17$ ) and  $L=0.59$ . The  $G$  value corresponding to the minimum MAD is 2.5. With the optimal parameter values, the EVI2 equation (Eq. (12)) becomes

$$\text{EVI2} = 2.5 \frac{N-R}{N+2.4R+1} \quad (15)$$

The  $R^2$  between EVI and EVI2 increases rapidly when  $L$  increases from 0 to 0.5, and then decreases for higher  $L$  values (Fig. 7). SAVI has a much higher  $R^2$  with EVI than NDVI, and the resulting  $R^2$  between EVI and EVI2 with the optimal parameters is 0.9986, very close to the maximum  $R^2$  values, indicating a strong linear relationship between these two indices.

According to Eq. (13), EVI2 can also be expressed as a function of the ratio of red to blue reflectances,  $c$ . As shown in Fig. 8, MAD between EVI and EVI2 is minimum when  $c=2.08$ , with the corresponding  $G$  equal to 2.5. The optimal  $c$  and  $G$  values render Eq. (13) to be the same as Eq. (15),

$$\text{EVI2} = 2.5 \frac{N-R}{N+(6-7.5/2.08)R+1} = 2.5 \frac{N-R}{N+2.4R+1}$$

Thus, the two alternative methods to develop the EVI2 equation coincided and resulted in the same EVI2 equation (Eq. (15)).

## 6. Evaluation of EVI–EVI2 consistency

### 6.1. Global comparisons

An example of EVI–EVI2 consistency on a global basis, evaluated with the MODIS 1 km data, is shown in Fig. 9 using the Jul 27–Aug 11, 2000 (DOY 209–224) composite period when vegetation photosynthesis is most active in summer for the Northern Hemisphere. The global EVI2 image exhibits similar values and spatial patterns of global vegetation conditions as the EVI image (Fig. 9a, b), with both VIs depicting eastern North America, northern South America, and parts of the East Asia with the highest VI values, and Europe and North Asia with intermediate VI values. The NDVI image is significantly different from the EVI and EVI2 images as most NDVI values over vegetated areas are very high, making it difficult to discriminate vegetation differences in forested areas (Fig. 9c). The NDVI image also seems greener than the EVI images over sparsely vegetated areas, such as the southwest U.S., South Africa, Australia and central Asia, since NDVI values are evidently larger than the EVI and EVI2 values over these areas.

The overall difference between EVI and EVI2 is small, with most of the difference between  $-0.02$  and  $0.02$  (Fig. 9d). Over some tropical areas, such as south Asia, the west coast of Africa, and South America, EVI values are slightly larger than EVI2 values ( $\sim 0.03$ ), possibly caused

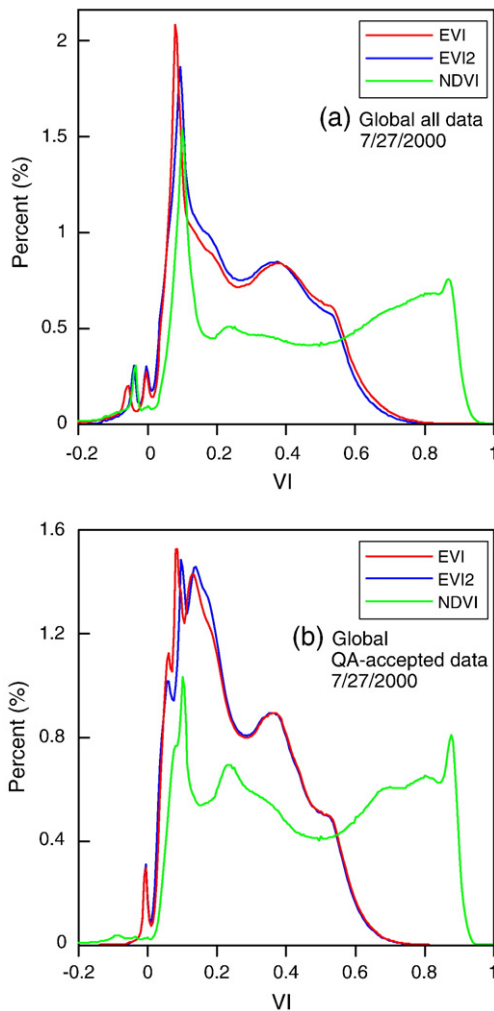


**Fig. 10.** Comparison of MODIS EVI, EVI2 and NDVI histograms of the global images shown in Fig. 9, (a) using global data, (b) using QA-accepted data. The sample interval of VI values is 0.0050.

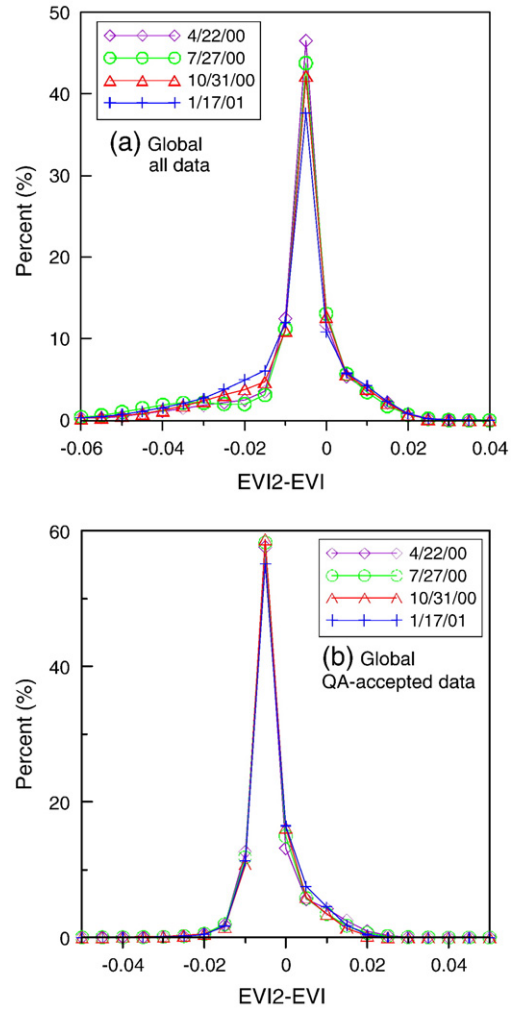


**Fig. 11.** Histograms of the difference between EVI and EVI2 over four composite periods in difference seasons, (a) using global data, and (b) using QA-accepted data. The sample interval is 0.0050. Each 16-day period is labeled by the beginning date of the period.

by the presence of residual mixed clouds in these areas, which result in blue reflectance and EVI artifacts. In some parts of sparsely vegetated desert areas, such as North Africa and central Australia, the EVI2 values are slightly larger than EVI values ( $0.01$ – $0.02$ ), which are caused by the higher blue/red ratios or  $c$  values ( $\sim 2.7$ ) than the value ( $2.08$ ) used in the EVI2 equation (Eq. (13)).

Histograms of the global images (Fig. 9) for (1) all global data and (2) only QA-accepted data cases are shown in Fig. 10. The global NDVI histogram has two peaks, at  $0.1$  and  $0.87$ . The rapid decrease in the NDVI frequency beyond  $0.87$  can be explained by the saturation effects of NDVI shown in Fig. 9c. In contrast, the histograms of global EVI and EVI2 have one prominent peak, near  $0.1$ , with a secondary peak at  $0.38$ . The EVI and EVI2 frequencies distribute more normally than the NDVI histogram with a more gradual decrease in frequencies from  $0.84\%$  at  $0.38$  to  $0.01\%$  at  $0.79$ , allowing more distinct discrimination of vegetated surfaces (Fig. 10a). The EVI frequency is slightly greater than the EVI2 frequency for VI values larger than  $0.4$ , and is slightly less than the EVI2 frequency for VI values between  $0.1$  and  $0.4$ . This disagreement is caused by the relatively high blue reflectances in pixels with aerosol, cloud, or snow. When only QA-accepted data are used, the histograms of EVI and EVI2 match very well, with only minor disagreements between  $0.06$  and  $0.21$  (Fig. 10b). The peak of the EVI2 histogram shifts slightly to higher values compared with the peak of the EVI histogram. These disagreements correspond to the slight higher EVI2 values in some parts of sparsely vegetated desert areas, such as North Africa and central Australia (Fig. 9d),

Histograms of the difference between EVI and EVI2 (EVI2 minus EVI) for all data and QA-accepted data cases, in four composite periods representing difference seasons are shown in Fig. 11. The EVI2–EVI differences, using all global data across four seasons, are mostly between  $-0.06$  and  $0.02$  (Fig. 11a). Seasonal variations in the EVI2–EVI differences are insignificant with 88.8% of the differences within  $\pm 0.02$  for the April composite period, and 84.7% for the July composite period. On average, 87.4% of the differences are within  $\pm 0.02$  in all 24 composite periods from Feb. 18, 2000 to Feb. 18, 2001, and 43.4% of the differences occur in the interval centered at  $-0.0050$ , i.e.  $(-0.0075, -0.0025)$ . When only QA-accepted data are used, 99.2% of the differences are between  $-0.02$  and  $0.02$ , on average, for all 24 composite periods, with the EVI2–EVI difference histograms almost seasonally independent (Fig. 11b). 57.1% of the differences occur in the interval centered at  $-0.0050$ . The modes of the difference histograms indicate the amplitude of the EVI2 is slightly smaller than the amplitude of EVI, on the order of 0.0050.

For the case of QA-accepted data where atmospheric influences are insignificant and mixed clouds, snow and ice are excluded, the small differences between EVI and EVI2 (within  $\pm 0.02$ ) are attributed to the intrinsic variation of the blue band over these land surfaces, to which EVI responds. For the global case, 9.8% of pixels in the 24 global 16-day composite images have EVI2–EVI differences between  $-0.06$  and  $-0.02$  (Fig. 11a). These differences are not likely caused by intrinsic

variations of the blue band over the land surface, but are mostly attributed to the residual variations of atmospheric conditions including aerosol and clouds or the presence of snow/ice at a subpixel scale, since the intrinsic variation of blue band over snow/ice-free surface is only responsible for EVI2–EVI differences within  $\pm 0.02$ . So the seasonal variations of atmospheric conditions and snow/ice are responsible for the seasonal variation of the EVI2–EVI differences. The frequencies for EVI2–EVI differences larger than  $+0.02$  are extremely low for both the QA-accepted and whole global data cases since the presence of aerosol/clouds and snow/ice can only increase the EVI values relative to the more aerosol sensitive EVI2 values (Fig. 11).

## 6.2. Transect comparisons

In order to evaluate the spatial differences among EVI, NDVI and EVI2 values, four continental-scale transects are sampled from the global VI images, and their locations are shown in Fig. 9a. Each transect includes sparse to densely vegetated regions to encompass a wide range of VI values. The land cover of the North America transect varies from grassland in the northwest, to woody savanna, with mixed forest and deciduous broadleaf forest appearing at the end or southeast portion of the transect. All of the vegetation indices increase gradually from the grassland area to the forested portions of the transect (Fig. 12a). The differences between EVI and EVI2 values are

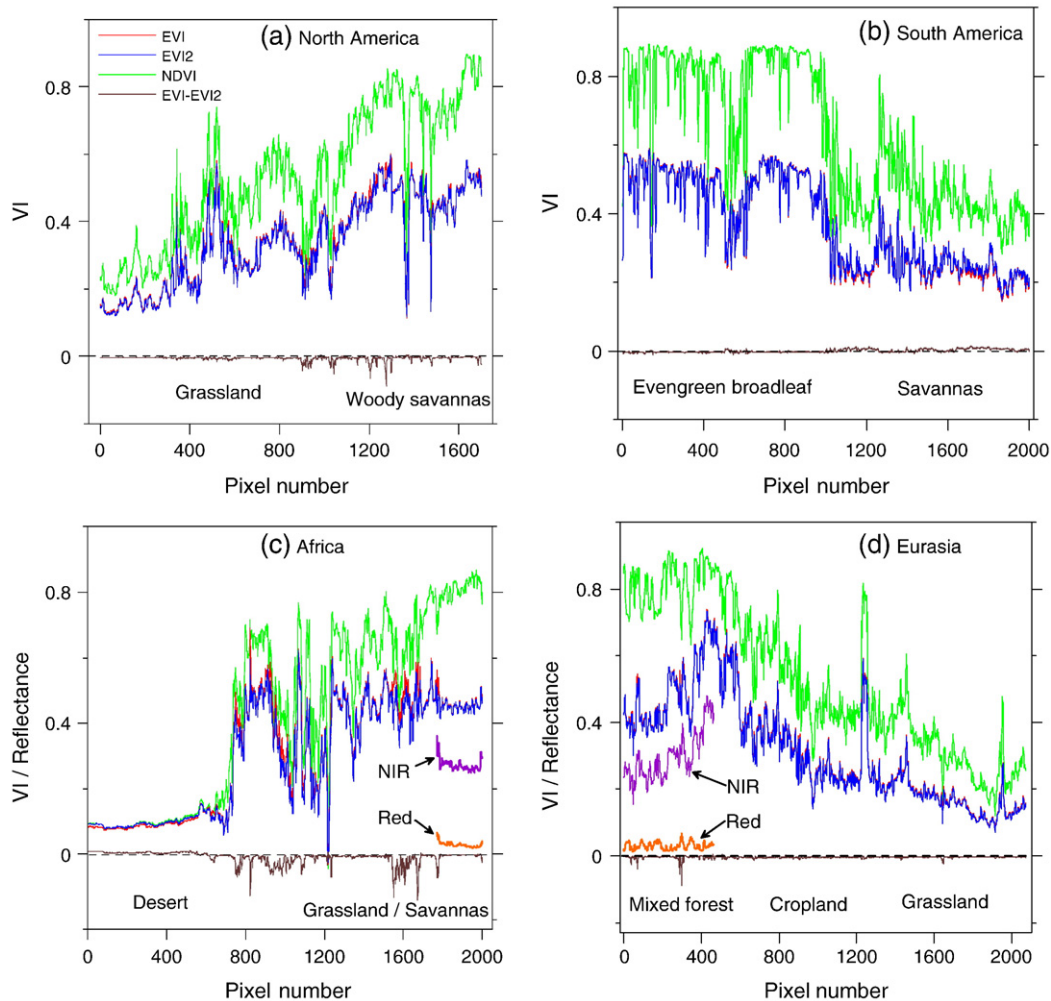


**Fig. 12.** Transects of 1 km, 16-day composite MODIS EVI, EVI2, NDVI and EVI2 minus EVI for the Jul 27–Aug 11, 2000 composite period. (a) North America transect, (b) South America transect, (c) Africa transect, and (d) Eurasia transect. The legends of (b), (c) and (d) are the same as (a). The locations of the four transects are shown in Fig. 9a by yellow lines. Each transect starts in the northwest side and ends in the southeast side. Different trends between the NDVI and EVI/EVI2 transects can be found at the end of the Africa transect and the beginning of the Eurasia transect, and the corresponding red and NIR reflectances are plotted to show the different sensitivities of NDVI and EVI/EVI2 to red and NIR reflectances.

generally small, except for a few pixels with differences exceeding 0.02. The South America transect encompasses wet evergreen broad-leaf forests in the northwest part of the transect, to savannas and mixed cropland in the southwest portion of the transect (Fig. 12b). The differences between the two indices are very small across the transect, mostly less than 0.005.

Differences between EVI and EVI2 are very small in the northern part of the Africa transect, in the Sahara desert (Fig. 12c). The land cover over the remaining transect varies gradually from grassland, savanna, to woody savanna. The EVI2 values are evidently lower than EVI values for certain locations along this transect. These differences generally occur in cases when the ratio of red reflectance to blue reflectance becomes closer to 1, indicating an abnormally stronger blue signal, possibly caused by cloud or aerosols. The land cover of the Eurasia transect changes from mixed forest towards the northwest, to cropland in middle, and grassland in the southeast and the differences between EVI and EVI2 are close to 0, except for a few pixels (Fig. 12d).

EVI2 generally tracks EVI very well within the four transects, while NDVI has distinct profile differences relative to both EVIs (Fig. 12). Towards the southern end of the Africa transect in the wooded savanna, NDVI increases dramatically while EVI and EVI2 show no apparent change or slight decrease (Fig. 12c). The increase of NDVI

results from the slight decrease of the red reflectance from 0.06 to 0.03 since the NIR reflectance decreases also, from 0.33 to 0.25. In the northern, mixed forest, portion of the Eurasia transect, EVI and EVI2 increase significantly as the NIR reflectance increases from 0.2 to 0.46, while NDVI shows little variation and becomes saturated (Fig. 12d). The different patterns and behavior of vegetation indices can be explained by their relative sensitivities to red and NIR reflectances since EVI is more sensitive to NIR reflectances while NDVI is very sensitive to red reflectances (Huete et al., 1997).

### 6.3. Time series and site comparisons

The EVI2 time series agree well with EVI time series at all sites (Fig. 13). The EVI is slightly larger than EVI2 at the peaks of the growing season at the Grand Morin and Chan Bai Shan sites. The NDVI profiles are distinct from the EVI and EVI2 profiles over the sites. Differences between NDVI and EVI are prominent at the Cascades/H.J. Andrews LTER site consisting of moist needleleaf forest. The low red reflectances at this site ( $\sim 0.01$ ) result in high NDVI values, but EVI and EVI2 values are moderate since the NIR reflectance is low, at  $\sim 0.2$ . The NDVI profile shows larger annual variation than the EVI and EVI2 profiles at this site due to the high sensitivity of NDVI to the red reflectance.

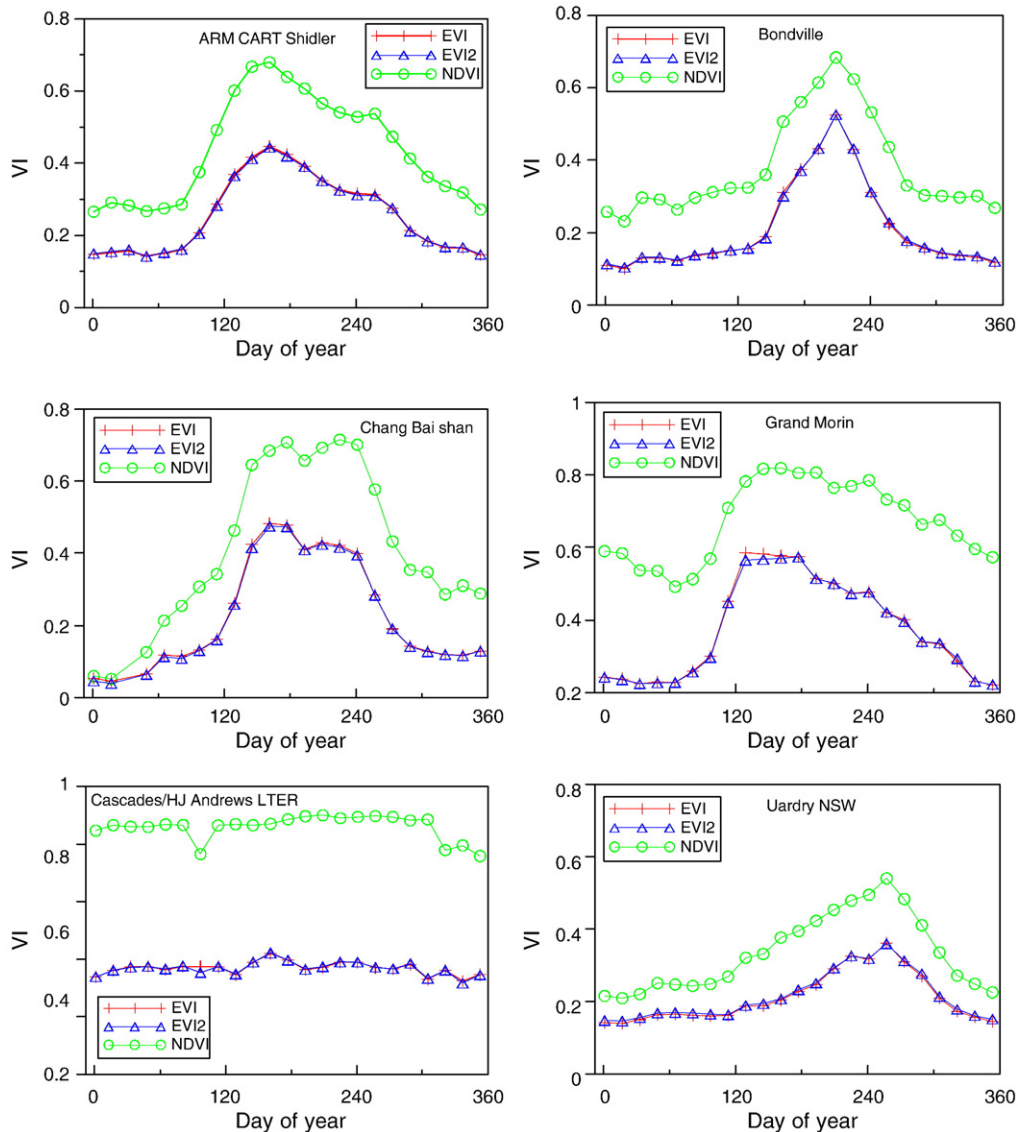
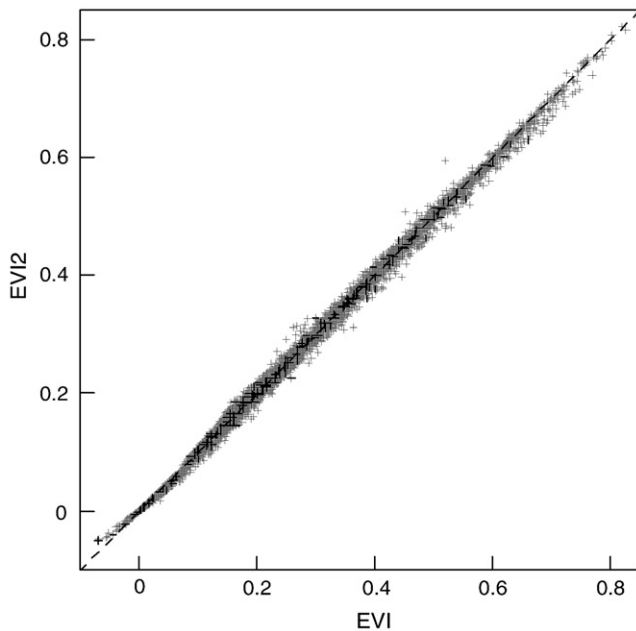


Fig. 13. Comparisons among MODIS EVI, EVI2 and NDVI time series at EOS land validation core sites. Vegetation types include grass (ARM CAR Shidler and Uardry NSW), crops (Bondville and Grand Morin), mountain forest (Chang Bai Shan), and moist needleleaf forest (Cascades/H.J. Andrews LTER).



**Fig. 14.** Cross-plot of EVI2 and EVI using QA-accepted MODIS 1 km, 16-day composite VI data over the 13 EOS Land Validation core sites from 2000 to 2006.

A cross-plot of EVI2 and EVI using all QA-accepted MODIS VI data over the 13 EOS Land Validation core sites shows a very close 1:1 relationship (Fig. 14). The average EVI2–EVI difference is  $-0.0007$ , with the MAD of  $0.0050$ , indicating insignificant differences between EVI and EVI2 for good quality observation conditions and across the wide variety of land cover conditions analyzed here. The linear relationship between EVI and EVI2 is a result of the moderate  $\beta$  value used in EVI2, which is between that used in SAVI ( $\beta=0$ ) and SASR ( $\beta=\pi/4$ ) equations, i.e., between the convex EVI–SAVI and concave EVI–SASR relationships, as shown in Fig. 2.

## 7. Discussion

Although EVI, a feedback-based soil and atmospheric resistant vegetation index, gained its heritage from SAVI and ARVI (Liu & Huete, 1995), it cannot be simply reduced to SAVI as a 2-band version of EVI since SAVI is less sensitive to greenness than EVI in high biomass regions as shown in Fig. 2. To enhance the sensitivity of SAVI in high biomass regions, a linearity-adjustment factor,  $\beta$ , is proposed and coupled with the soil-adjustment concept used in SAVI, resulting in the linear vegetation index (LVI). EVI2 takes the formula of LVI, but with optimized parameter values, obtained through calibration in the two-dimension parameter ( $L$ – $\beta$ ) space, such that the mean absolute difference between EVI and EVI2 is minimized using a global dataset consisting of QA-accepted reflectances over 40 sites and 6 years of MODIS VI, 16-day composites (Fig. 6). The 1:1 relationship between EVI and EVI2 suggests that EVI2 not only has an improved sensitivity over high biomass, relative to the SAVI, but also minimizes soil influences as in EVI.

It should be noted that  $L$ , as used in EVI2 (0.59), is slightly different from  $L$  in SAVI (0.5), indicating a discrepancy in the soil-adjustment factors. However, this is not a serious conflict, since for any  $L$  from 0.25 to 1, the soil background influences are considerably reduced in comparison to NDVI (case of  $L=0$ ) and Perpendicular Vegetation Index (PVI, case of  $L>100$ ) (Huete, 1988). SAVI was developed with only consideration of soil background influences. However, EVI was developed with consideration of both soil background and atmospheric influences. Several studies found the soil and atmospheric influences couple and interact each other (Huete & Liu, 1994; Liu &

Huete, 1995). So, the differences in soil-adjustment factors adopted by SAVI and EVI2 are mostly explained by soil-atmospheric interactions, which are only taken into account by EVI. The  $L$  in the EVI equation (Eq. (3)) should not be interpreted as an exclusive soil-adjustment factor as the  $L$  in SAVI and LVI equations (Eqs. (2) and (12)), since EVI handles soil and atmosphere interactions. This interaction is decoupled in LVI equation, which shows the interaction between  $L$  and  $\beta$  in the last term of the equation's denominator, i.e.  $L/(1-\tan(\beta))$ .

The alternative strategy for EVI2 development was to decompose the original EVI equation to eliminate the blue band by assuming that the blue reflectances can be expressed as a function of the red reflectances. In fact, the decomposition method can be considered as a special case of the LVI method. The optimization of  $c$  in Eq. (13) is equivalent to the optimization of  $\beta$  in the LVI equation (Eq. (12)) under the constraint,  $L=1-\tan(\beta)$ , which represents a curve in the  $L$ – $\beta$  space.

The choice of the parameter values used for EVI2 is dependent on the average ratio of the red to blue band reflectances, and thus is partly dependent on the spectral characteristics of the sensors. EVI2 is developed here, based on MODIS data. For other sensors with different red or blue spectral response functions, the average ratio of the red to blue band may be different, so the relationship between EVI and EVI2 may vary slightly from one sensor to another.

The close relationship between EVI and EVI2 is associated with the close and stable relationship between the red and blue reflectances over terrestrial surfaces, when minimal atmospheric effects and no snow and ice exist (Fig. 4). Since the blue band provides none or very little additional biophysical information than the red band, EVI2, without the blue band, can retain the merits of EVI, except for the aerosol resistance function. Thus, larger differences ( $>0.02$ ) between EVI and EVI2 are mostly due to residual aerosol and cloud influences that remain after atmosphere correction of MODIS data.

EVI2, in turn, can provide a reliable reference for EVI to assess the atmospheric self-correction made by using a blue band in the EVI equation. In this study, EVI appears useful in reducing atmosphere influences on 9.8% of pixels globally, resulting in increases in the EVI values mostly between 0.02 and 0.06, compared with the corresponding EVI2 values. Generally, the spatial extent and frequency of atmospheric self-corrections by EVI are fairly limited, partly due to improvements in atmosphere corrections by the MODIS (MOD09) surface reflectance product (Vermette et al., 2002), and by the MODIS VI compositing algorithm which attempts to select the best observation within a 16-day period.

It is interesting that different, even opposite, patterns and behaviors are observed between NDVI and EVI/EVI2 over woody savannas and mixed forest (Fig. 12 c and d). Many studies found that NDVI becomes saturated over highly vegetated areas and does not respond to variation of NIR reflectances when the red reflectance is low (Carlson & Ripley, 1997; Gitelson, 2004; Huete et al., 1997; Wardlow et al., 2007). However, EVI and EVI2 remain sensitive to variation of the NIR reflectances when the red reflectance is low (Fig. 12d). The NDVI histogram shows a peak at high NDVI values associated with saturation, but the EVI2 histogram is more normally distributed (Fig. 10). These findings suggest that AVHRR EVI2 would reveal different vegetation dynamics in comparison with the current AVHRR NDVI dataset especially when the red reflectance is low and NDVI becomes saturated.

This study is based on 1-km resolution MODIS data. But the justification and application of EVI2 is not limited to this resolution since a wide range of reflectances is included and data of smaller resolution should be within the reflectance range as shown in Figs. 3 and 4. As LVI can be calibrated to EVI, its linearity-adjustment capability would enable the LVI to be coupled to specific vegetation biophysical parameters, resulting in more linear relationships, particularly when remotely sensed data and the corresponding ground biophysical parameters are measured together.

## 8. Summary

In this study, a 2-band EVI without a blue band is developed and evaluated using global-, land cover specific-, and local scale MODIS data. EVI2 can be used as an exact substitute of EVI for good observations, i.e., good QA pixels that contain no cloud or snow and are atmospherically corrected over low aerosol quantity. The challenge in the development of an EVI2 is not only to retain the soil-noise adjustment function, but also to maintain the improved sensitivity and linearity in high biomass regions (non-saturation) seen in EVI. To achieve these goals, the linear vegetation index (LVI) was proposed, which incorporates the soil-adjustment factor of SAVI with a linearity-adjustment factor,  $\beta$ . It is through  $\beta$ , that the sensitivity of an index can be improved in high biomass regions and become comparable with EVI, allowing the relationship between EVI and LVI to become more linear.

The similarity between EVI and EVI2 was analyzed and validated at the local and global scales. Global EVI2 images show very similar patterns as global EVI images and the differences between them were insignificant using QA-acceptable data, with nearly all pixels within  $\pm 0.02$ . When aerosol or residual clouds are present, EVI is generally larger than EVI2, due to the aerosol resistance property of EVI. The consistency between EVI and EVI2 across various land cover types demonstrated that their similarity was independent of land cover. Time series (temporal) analysis further revealed their similarity was seasonally independent.

EVI2 can be used for sensors without a blue band, such as the AVHRR and ASTER instruments, to produce an EVI-like vegetation index, complementary to NDVI. Our findings suggest that an AVHRR-based EVI2 may reveal different vegetation dynamics in comparison with the current AVHRR NDVI dataset especially when red reflectances are low and NDVI becomes saturated. The relationships and continuity among EVI2 values derived from different sensors remain to be studied. As MODIS NDVI is significantly higher than AVHRR NDVI (Huete et al., 2002; Miura et al., 2006), the EVI2 of these two sensors may also differ and cross-sensor calibration of reflectances should be conducted before comparing an AVHRR EVI2 with MODIS EVI/EVI2.

## Acknowledgements

This work was supported by NASA MODIS contract #NNG04HZ20C (A. Huete, P.I.), NASA grant #NNG04GJ22G for the assessment of Vegetation Index Environmental Data Records with NPP VIIRS (J. Privette, P.I.), and NASA EOS grant NNG04GL88G (T. Miura, P.I.).

## Appendix A

Derivation of LVI:

$$\begin{aligned} \text{LVI} &= G' [\tan(\alpha + \beta) - \tan\beta] \\ &= G' \frac{\tan\alpha + \tan\alpha \tan^2\beta}{1 - \tan\alpha \tan\beta} = G' \sec^2\beta \frac{\tan\alpha}{1 - \tan\alpha \tan\beta} \end{aligned} \quad (\text{A} - 1)$$

According to Eqs. (5) and (6),

$$\tan\alpha = \frac{N-R}{N+R+L} \quad (\text{A} - 2)$$

By substitute Eq. (A-2) into Eq. (A-1), LVI can be expressed as a function of  $N$  and  $R$ .

$$\begin{aligned} \text{LVI} &= G' \sec^2\beta \frac{N-R}{N(1-\tan\beta) + R(1+\tan\beta) + L} \\ &= G \frac{N-R}{N + R \tan(\pi/4 + \beta) + L / (1 - \tan\beta)} \end{aligned}$$

where

$$G = \frac{G' \sec^2\beta}{1 - \tan\beta}$$

## References

- Ahl, D. E., Gower, S. T., Burrows, S. N., Shabanow, N. V., Myneni, R. B., & Knyazikhin, Y. (2006). Monitoring spring canopy phenology of a deciduous broadleaf forest using MODIS. *Remote Sensing of Environment*, 104, 88–95.
- Baret, F., & Guyot, G. (1991). Potentials and limits of vegetation indices for LAI and APAR assessment. *Remote Sensing of Environment*, 35, 161–173.
- Baret, F., Guyot, G., & Major, D. (1989). TSAVI: A vegetation index which minimizes soil brightness effects on LAI and APAR estimation. *12th Canadian symposium on remote sensing and IGARSS'90, Vancouver, Canada, 10–14 July 1989* (pp. 1355–1358).
- Bausch, W. C. (1993). Soil background effects on reflectance-based crop coefficients for corn. *Remote Sensing of Environment*, 46, 213–222.
- Ben-Ze'ev, E., Karnieli, A., Agam, N., Kaufman, Y., & Holben, B. (2006). Assessing vegetation condition in the presence of biomass burning smoke by applying the aerosol-free vegetation index (AFRI) on MODIS. *International Journal of Remote Sensing*, 27, 3203–3221.
- Blackburn, A. G. (1998). Quantifying chlorophylls and carotenoids at leaf and canopy scales: An evaluation of some hyperspectral approaches. *Remote Sensing of Environment*, 66, 273–285.
- Boegh, E., Soegaard, H., Broge, N., Hasager, C. B., Jensen, N. O., Schelde, K., et al. (2002). Airborne multispectral data for quantifying leaf area index, nitrogen concentration, and photosynthetic efficiency in agriculture. *Remote Sensing of Environment*, 81, 179–193.
- Brown, E. M., Pinzón, E. J., Didan, K., Morisette, T. J., & Tucker, J. C. (2006). Evaluation of the consistency of long-term NDVI time series derived from AVHRR, SPOT-Vegetation, SeaWiFS, MODIS, and Landsat ETM+ sensors. *IEEE Transactions on Geoscience and Remote Sensing*, 44, 1787–1793.
- Carlson, T. N., & Ripley, D. A. (1997). On the relation between NDVI, fractional vegetation cover, and leaf area index. *Remote Sensing of Environment*, 62, 241–252.
- Che, N., & Price, C. J. (1992). Survey of radiometric calibration results and methods for visible and near infrared channels of NOAA-7, -9 and -11 AVHRRs. *Remote Sensing of Environment*, 41, 19–27.
- Chen, J. M., & Cihlar, J. (1996). Retrieving leaf area index of boreal conifer forests using Landsat TM images. *Remote Sensing of Environment*, 55, 153–162.
- Chen, X., Vierling, L., Rowell, E., & DeFelicis, T. (2004). Using lidar and effective LAI data to evaluate IKONOS and Landsat 7 ETM+ vegetation cover estimates in a ponderosa pine forest. *Remote Sensing of Environment*, 91, 14–26.
- Clevers, J. G. P. W. (1999). The use of imaging spectrometry for agricultural applications. *ISPRS Journal of Photogrammetry and Remote Sensing*, 54, 299–304.
- Defries, R. S., & Belward, A. S. (2000). Global and regional land cover characterization from satellite data. *International Journal of Remote Sensing*, 21, 1083–1092.
- Deng, F., Su, G., & Liu, C. (2007). Seasonal variation of MODIS vegetation indices and their statistical relationship with climate over the subtropic evergreen forest in Zhejiang, China. *IEEE Geoscience and Remote Sensing Letters*, 4(2), 236–240.
- Di Bella, C. M., Paruelo, J. M., Becerra, J. E., Bacour, C., & Baret, F. (2004). Effect of senescent leaves on NDVI-based estimates of f APAR: experimental and modelling evidences. *International Journal of Remote Sensing*, 25, 5415–5427.
- Didan, K., & Huete, A. R. (2006). *MODIS vegetation index product series collection 5 change summary*. Available online at [http://modland.nascom.nasa.gov/QA\\_WWWW/forPage/MOD13\\_VI\\_C5\\_Changes\\_Document\\_06\\_28\\_06.pdf](http://modland.nascom.nasa.gov/QA_WWWW/forPage/MOD13_VI_C5_Changes_Document_06_28_06.pdf)
- Elvidge, C. D., & Lyon, R. J. P. (1985). Influence of rock-soil spectral variation on the assessment of green biomass. *Remote Sensing of Environment*, 17, 265–279.
- Fensholt, R., Sandholt, I., & Stisen, S. (2006). Evaluating MODIS, MERIS, and VEGETATION indices using in situ measurements in a semiarid environment. *IEEE Transactions on Geoscience and Remote Sensing*, 44, 1774–1786.
- Gallo, K. J., Reed, B., Eidsenshink, J., & Dwyer, J. (2005). Multi-platform comparisons of MODIS and AVHRR normalized difference index data. *Remote Sensing of Environment*, 99, 221–231.
- Gilbert, M. A., González-Piqueras, J., García-Haro, F. J., & Meliá, J. (2002). A generalized soil-adjusted vegetation index. *Remote Sensing of Environment*, 82, 303–310.
- Gitelson, A. A. (2004). Wide dynamic range vegetation index for remote quantification of biophysical characteristics of vegetation. *Journal of Plant Physiology*, 161, 165–173.
- Gitelson, A. A., & Kaufman, J. Y. (1998). MODIS NDVI optimization to fit the AVHRR data series—Spectral consideration. *Remote Sensing of Environment*, 66, 343–350.
- Gitelson, A. A., Vina, A., Ciganda, V., Rundquist, C. D., & Arkebauer, J. T. (2005). Remote estimation of canopy chlorophyll content in crops. *Geophysical Research Letters*, 32, L08403. doi:10.1029/2005GL022688.
- Günther, P. K., & Maier, W. S. (2007). AVHRR compatible vegetation index derived from MERIS data. *International Journal of Remote Sensing*, 28, 693–708.
- Gutman, G., & Ignatov, A. (1998). The derivation of the green vegetation fraction from NOAA/AVHRR data for use in numerical weather prediction models. *International Journal of Remote Sensing*, 19, 1533–1543.
- Heumann, W. B., Seaquist, W. J., Eklundh, L., & Jonsson, P. (2007). AVHRR derived phenological change in the Sahel and Soudan, Africa, 1982–2005. *Remote Sensing of Environment*, 108, 385–392.
- Houborg, R., Soegaard, H., & Boegh, E. (2007). Combining vegetation index and model inversion methods for the extraction of key vegetation biophysical parameters using Terra and Aqua MODIS reflectance data. *Remote Sensing of Environment*, 106, 39–58.
- Huete, A. R. (1988). A soil-adjusted vegetation index (SAVI). *Remote Sensing of Environment*, 25, 295–309.
- Huete, A. R., & Liu, H. Q. (1994). An error and sensitivity analysis of the atmospheric- and soil-correcting variants of the NDVI for the MODIS-EOS. *IEEE Transactions on Geoscience and Remote Sensing*, 32, 897–905.
- Huete, A. R., Jackson, R. D., & Post, D. F. (1985). Spectral response of a plant canopy with different soil backgrounds. *Remote Sensing of Environment*, 17, 37–53.

- Huete, A. R., Liu, H. Q., Batchily, K., & Leeuwen van, W. (1997). A comparison of vegetation indices over a global set of TM images for EOS-MODIS. *Remote Sensing of Environment*, 59, 440–451.
- Huete, A. R., Didan, K., Miura, T., Rodriguez, E. P., Gao, X., & Ferreira, L. G. (2002). Overview of the radiometric and biophysical performance of the MODIS vegetation indices. *Remote Sensing of Environment*, 83, 195–213.
- Huete, A. R., Didan, K., Shimabukuro, Y. E., Ratana, P., Saleska, C. R., Hutyrá, L. R., et al. (2006). Amazon rainforests green-up with sunlight in dry season. *Geophysical Research Letters*, 33, L06405. doi:10.1029/2005GL025583.
- Jiang, Z., Huete, A. R., Chen, J., Chen, Y., Li, J., Yan, G., et al. (2006). Analysis of NDVI and scaled difference vegetation index retrievals of vegetation fraction. *Remote Sensing of Environment*, 101, 366–378.
- Jiang, Z., Huete, A. R., Li, J., & Chen, Y. (2006). An analysis of angle-based with ratio-based vegetation indices. *IEEE Transactions on Geoscience and Remote Sensing*, 44, 2506–2513.
- Karnieli, A., Kuafman, Y. J., Remer, L., & Wald, A. (2001). AFRI-aerosol free vegetation index. *Remote Sensing of Environment*, 77, 10–21.
- Kaufman, Y. J., & Tanré, D. (1992). Atmospherically resistant vegetation index (ARVI) for EOS-MODIS. *IEEE Transactions on Geoscience and Remote Sensing*, 30, 261–270.
- Kaufman, Y. J., & Holben, B. N. (1993). Calibration of the AVHRR visible and near-IR bands by atmospheric scattering, ocean glint and desert reflection. *International Journal of Remote Sensing*, 14, 21–52.
- Kaufman, Y. J., Wald, A. E., Remer, L. A., Gao, B. -C., Li, R. -R., & Luke, F. (1997). The MODIS 2.1-mm band correlation with visible reflectance for use in remote sensing of aerosol. *IEEE Transactions on Geoscience and Remote Sensing*, 35, 1286–1298.
- Liu, H. Q., & Huete, A. (1995). A feedback based modification of the NDVI to minimize canopy background and atmospheric noise. *IEEE Transactions on Geoscience and Remote Sensing*, 33, 457–465.
- Los, S. (1993). Calibration adjustment of the NOAA AVHRR normalized difference vegetation index without recourse to component Channel 1 and 2 data. *International Journal of Remote Sensing*, 14, 1907–1917.
- Mitchell, R. M., O'Brien, D. M., Edwards, M., Elsum, C. C., & Graetz, R. D. (1997). Selection and initial characterization of a bright calibration site in the Strzelecki Desert, South Australia. *Canadian Journal of Remote Sensing*, 23, 342–353.
- Miura, T., Huete, A. R., & van Leeuwen, W. J. D. (1998). Vegetation detection through smoke-filled AVHRR images: An assessment using MODIS band passes. *Journal of Geophysical Research*, 103(D24), 32,001–32,011.
- Miura, T., Huete, A. R., & Yoshioka, H. (2006). An empirical investigation of cross-sensor relationships of NDVI and red/near-infrared reflectance using EO-1 Hyperion data. *Remote Sensing of Environment*, 100, 223–236.
- Morissette, J. T., Privette, J. L., & Justice, C. O. (2002). A framework for the validation of MODIS Land products. *Remote Sensing of Environment*, 83, 77–96.
- Myneni, B. R., Keeling, D. C., Tucker, J. C., Asrar, G., & Nemani, R. R. (1997). Increased plant growth in the northern high latitudes from 1981 to 1991. *Nature*, 386(17), 698–702.
- Myneni, B. R., Nemani, R. R., & Running, W. S. (1997). Estimation of global leaf area and absorbed PAR using radiative transfer models. *IEEE Transactions on Geoscience and Remote Sensing*, 35, 1380–1393.
- Nagler, P. L., Cleverly, J., Glenn, E., Lampkin, D., Huete, A. R., & Wan, Z. (2005). Predicting riparian evapotranspiration from MODIS vegetation indices and meteorological data. *Remote Sensing of Environment*, 94, 17–30.
- Privette, J. L., Myneni, R. B., Knyazikhin, Y., Mukelabai, M., Roberts, G., Tian, Y., et al. (2002). Early spatial and temporal validation of MODIS LAI product in the Southern Africa Kalahari. *Remote Sensing of Environment*, 83, 232–243.
- Qi, J., Chehbouni, A., Huete, A. R., Kerr, H. Y., & Sorooshian, S. (1994). A modified soil adjusted vegetation index. *Remote Sensing of Environment*, 48, 119–126.
- Rahman, A. F., Sims, D. A., Cordova, V. D., & El-Masri, B. Z. (2005). Potential of MODIS EVI and surface temperature for directly estimating per-pixel ecosystem C fluxes. *Geophysical Research Letters*, 32, L19404. doi:10.1029/2005GL024127.
- Richardson, A. J., & Wiegand, C. L. (1977). Distinguishing vegetation from soil background information. *Photogrammetric Engineering and Remote Sensing*, 43, 1541–1552.
- Roderick, M., Smith, R., & Lodwick, G. (1996). Calibrating long-term AVHRR-derived NDVI imagery. *Remote Sensing of Environment*, 58, 1–12.
- Rondeaux, G., & Baret, F. (1996). Optimization of soil-induced vegetation indices. *Remote Sensing of Environment*, 55, 95–107.
- Saleska, R. S., Didan, K., Huete, R. A., & da Rocha, R. H. (2007). Amazon forests green-up during 2005 drought. *Science*, 318, 612.
- Sims, D. A., Rahman, A. F., Cordova, V. D., El-Masri, B. Z., Baldocchi, D. D., Flanagan, L. B., et al. (2006). On the use of MODIS EVI to assess gross primary productivity of North American ecosystems. *Journal of Geophysical Research*, 111, G04015. doi:10.1029/2006JG000162.
- Sims, D. A., Rahman, A. F., Cordova, V. D., El-Masri, B. Z., Baldocchi, D. D., Bolstad, P. V., et al. (2008). A new model of gross primary productivity for North American ecosystems based solely on the enhanced vegetation index and land surface temperature from MODIS. *Remote Sensing of Environment*, 112, 1633–1646.
- Steven, D. M., Malthus, J. T., Baret, F., Xu, H., & Chopping, J. M. (2003). Intercalibration of vegetation indices from different sensor systems. *Remote Sensing of Environment*, 88, 412–422.
- Suzuki, K., Masuda, K., & Dye, D. G. (2007). Interannual covariability between actual evapotranspiration and PAL and GIMMS NDVIs of northern Asia. *Remote Sensing of Environment*, 106, 387–398.
- Townshend, J. R. G. (1994). Global data sets for land applications from the advanced very high resolution radiometer: An introduction. *International Journal of Remote Sensing*, 15, 3319–3332.
- Tucker, J. C., Fung, I. Y., Keeling, C. D., & Gammon, R. H. (1986). Relationship between atmospheric CO<sub>2</sub> variations and a satellite-derived vegetation index. *Nature*, 319, 195–199.
- Tucker, J. C., Slayback, A. D., Pinzon, E. J., Los, O. S., Myneni, B. R., & Taylor, G. M. (2001). Higher northern latitude normalized difference vegetation index and growing season trends from 1982 to 1999. *International Journal of Biometeorology*, 45, 184–190.
- Tucker, J. C., Pinzon, E. J., Brown, E. M., Slayback, A. D., Pak, W. E., Mahoney, R., et al. (2005). An extended AVHRR 8-km NDVI dataset compatible with MODIS and SPOT vegetation NDVI data. *International Journal of Remote Sensing*, 26, 4485–4498.
- Ünsalan, C., & Boyer, K. L. (2004). Linearized vegetation indices based on a formal statistical framework. *IEEE Transactions on Geoscience and Remote Sensing*, 42, 1575–1585.
- Vaipopoulos, D., Skianis, G. A., & Nikolakopoulos, K. (2004). The contribution of probability theory in assessing the efficiency of two frequently used vegetation indices. *International Journal of Remote Sensing*, 25, 4219–4236.
- van Leeuwen, J. D. W., Orr, J. B., Marsh, E. S., & Herrmann, M. S. (2006). Multi-sensor NDVI data continuity: uncertainties and implications for vegetation monitoring applications. *Remote Sensing of Environment*, 100, 67–81.
- Vermote, E. F., El Saleous, N. E., & Justice, C. O. (2002). Atmospheric correction of MODIS data in the visible to middle infrared: first results. *Remote Sensing of Environment*, 83, 97–111.
- Wardlow, B. D., Egbert, S. L., & Kastens, J. H. (2007). Analysis of time-series MODIS 250 m vegetation index data for crop classification in the U.S. Central Great Plains. *Remote Sensing of Environment*, 108, 290–310.
- Waring, R. H., Coops, N. C., Fan, W., & Nightingale, J. M. (2006). MODIS enhanced vegetation index predicts tree species richness across forested ecoregions in the contiguous U.S.A.. *Remote Sensing of Environment*, 103, 218–226.
- Xiao, X., Braswell, B., Zhang, Q., Boles, S., Frohling, S., & Moore, B. (2003). Sensitivity of vegetation indices to atmospheric aerosols: Continental-scale observations in Northern Asia. *Remote Sensing of Environment*, 84, 385–392.
- Xiao, X., Hagen, S., Zhang, Q., Keller, M., & Moore, B. (2006). Detecting leaf phenology of seasonally moist tropical forests in South America with multi-temporal MODIS images. *Remote Sensing of Environment*, 103, 465–473.
- Xiao, X., Hollinger, D., Aber, J., Goltz, M., Davidson, E. A., Zhang, Q., et al. (2004). Satellite-based modeling of gross primary production in an evergreen needleleaf forest. *Remote Sensing of Environment*, 89, 519–534.
- Yoshioka, H., Miura, T., & Huete, A. R. (2003). An isoline-based translation technique of spectral vegetation index using EO-1 hyperion data. *IEEE Transactions on Geoscience and Remote Sensing*, 41, 1363–1372.
- Zeng, X., Dichinson, E. R., Walker, A., & Shaikh, M. (2000). Derivation and evaluation of global 1-km fractional vegetation cover data for land modeling. *Journal of Applied Meteorology*, 39, 826–839.
- Zhang, X., Friedl, M. A., Schaaf, C. B., Strahler, A. H., Hodges, J. C. F., Gao, F., et al. (2003). Monitoring vegetation phenology using MODIS. *Remote Sensing of Environment*, 84, 471–475.